JOURNAL OF GEOPHYSICAL RESEARCH, VOL. 113, B05405, doi:10.1029/2007JB005247, 2008

Noise in GPS displacement measurements from Southern California and Southern Nevada

John Langbein[1]

Received 26 June 2007; revised 30 November 2007; accepted 21 January 2008; published 16 May 2008.

[1] Time series of position changes estimated from data from 236 continuously recording GPS receivers operating in Southern California and Southern Nevada are evaluated for noise models that characterize their temporal correlations. The lengths of the time series range between 3.5 and 10 years. After adjusting these data for postseismic deformation, offsets, and annual periodicities, I find that about one-half of the time series have temporal correlations that are categorized as either flicker or random-walk noise. The remaining time series can be best categorized as either a combination of flicker and random-walk; power law noise; first-order Gauss-Markov plus random-walk noise; or power law plus broadband, seasonal noise. A variety of geodetic monuments are used in Southern California and Nevada, including deeply braced designs, cement piers, pins drilled in outcrop, and buildings. When I evaluate the noise for each time series in terms of an estimate of the standard error in velocity, I find that the sites with the smallest errors are those located in Nevada using deeply braced monuments. Sites that are installed within regions of active pumping, both for groundwater and oil, had the largest standard errors in velocity. Comparison of monument stability, as measured by standard error in rate, with average, annual rainfall nearby indicates a marginally significant correlation. In addition, even though regional filtering removed much of the common-mode signals in these time series, there still remains a common-mode seasonal signal which can and should be removed.

Citation: Langbein, J. (2008), Noise in GPS displacement measurements from Southern California and Southern Nevada, *J. Geophys. Res.*, *113*, B05405, doi:10.1029/2007JB005247.

1. Introduction

[2] Several papers, including *Langbein and Johnson* [1997], *Zhang et al.* [1997], *Mao et al.* [1999], *Williams et al.* [2004], and *Beavan* [2005], have demonstrated that daily, geodetic measurements of position or distance changes are temporally correlated rather than simply independent observations. The first-order effects of temporally correlated data have been summarized by *Johnson and Agnew* [1995], *Williams* [2003], and *Langbein* [2004]. They show that using models describing temporal correlations directly affects the estimates of the standard error of the rates that are derived by using least squares fitting a linear trend in time to the deformation time series. The model that describes the temporal correlations of the data is quantified in the data covariance matrix. The covariance matrix is used in conjunction with a function to fit, in a least squares sense, the temporal variations, including the rate, to the time series of the deformation data [e.g., *Menke*, 1984]. The covariance matrix represents the assumed noise processes of the data.

[3] The noise model for geodetic data has been modeled in the frequency domain as a combination of white noise, where the power density is independent of frequency, and a power law, f^{-n}, where f is frequency. Initial characterization of the power law process was done by *Langbein and Johnson* [1997] using two-color electronic distance meter (EDM) observations, and restricted the power law index, n, to be 2. They assumed that the temporally correlated process for noise was that of a random walk, which might characterize localized, random motions of the geodetic monument [*Wyatt*, 1982, 1989]. However, studies by *Zhang et al.* [1997] and *Mao et al.* [1999] of the time series of position changes measured by GPS suggested that the appropriate process for GPS was that of flicker noise, where $n = 1$.

[4] *Williams et al.* [2004] did a comprehensive analysis of over 400 GPS stations, and for those sites that are from regional networks and from which common-mode signals had been removed, the noise models for the data were best characterized by power law noise, where the index was between that of flicker and random walk. In many cases, since the $n \approx 1$, there was no compelling reason to reject the hypothesis of a flicker-noise process. In addition, *Williams et al.* [2004] explored the relationship between monument design and the level of noise. They concluded that the deeply braced monuments [*Wyatt et al.*, 1989; *Langbein et al.*, 1995] employed by the Southern California Integrated GPS Network (SCIGN) had less temporally correlated noise than other types of monuments used in that network. In addition,

[1]U.S. Geological Survey, Menlo Park, California, USA.

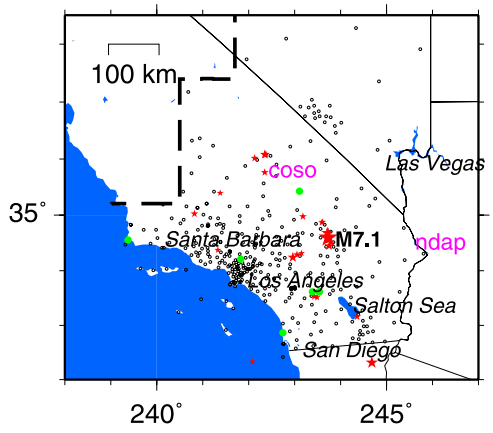

Figure 1. Locations of the GPS sites in Southern California and Nevada used in this study are shown as small circles. Larger, green dots denote fiducial stations used by SOPAC to construct a regional filter. Stars, with their size scaled to their magnitude, show the locations of $M > 5$ earthquakes in this region between 1996 and 2006. Of all the earthquakes, only the Hector Mine, M7.1 on 16 October 1999 and the M5.2 on 17 July 2001 near Coso produced significant offsets in the GPS observations.

the level of correlated noise from the Basin and Range Geodetic Network (BARGEN) was significantly less than the other three regional networks that they analyzed. The BARGEN network can be considered homogeneous in terms of monument type, all being deeply braced monuments; and environment, with all sites located in the desert with low erosion rates and low humidity, both factors that might lessen the effect of correlated noise.

[5] *Beavan* [2005] re-examined the monument stability problem by comparing the noise models derived from time series of position changes estimated from GPS measurements from massive, cement pillars used in New Zealand with results obtained from the three US regional networks analyzed by *Williams et al.* [2004]. He concluded that the correlated noise in the New Zealand data did not differ significantly from those of the US networks, which included a mix of monument types, including many deeply braced monuments.

[6] *Langbein* [2004] extended the possible set of noise models and re-examined the two-color EDM data discussed by *Langbein and Johnson* [1997]. In addition to the power law noise, he derived covariance matrices that incorporated Gauss-Markov processes, and band-passed filtered noise which could be used to characterize the seasonal component of noise found in many geodetic time series. In addition to the noise modeling, for the deterministic part of the analysis, which included rate, rate changes, offsets due to earthquakes or site maintenance, *Langbein et al.* [2006] extended the list of functions to characterize postseismic deformation, including Omori's Law, where displacement is proportional to $\log(1 + t/\tau)$ and an exponential decay, where displacement is proportional to $1-e^{-t/\tau}$.

[7] For the two-color EDM data, *Langbein* [2004] found that no single noise model satisfied all of the data. Rather, he found that all of the models described above were needed to characterize the noise in the EDM observations. In contrast to the noise models derived for GPS data by *Williams et al.* [2004], the noise in the EDM time series appears to be more complex. In part, this difference is due to the fact that the more complex noise models have not been applied to the GPS observations and, secondly, the EDM data provided, on average, a longer time series for which the longer period components of the noise could be resolved [*Williams et al.*, 2004; *Langbein*, 2004].

[8] This report tests whether the more complex noise models derived by *Langbein* [2004] provide a significantly better fit to the GPS observations than the power law model. In addition, since several years have elapsed since the *Williams et al.* [2004] study, the GPS time series used here are longer than those available to *Williams et al.* [2004]. Where *Williams et al.* [2004] used time series from the SCIGN array that, on average had 2.5 years of observation, this report restricts the length to greater than 3.9 years; The longer time series, which were not available to *Williams et al.* [2004], should help resolve the longer period components of the noise.

2. Data and Methods

[9] In this paper I restrict my analysis to the GPS sites located in Southern California and Southern Nevada, which constitute SCIGN and the southern part of BARGEN (or SBAR), respectively (Figure 1). These data (ftp://garner.ucsd.edu/pub/timeseries/) have been processed by the Scripps Orbit and Permanent Array Center (SOPAC) through January 2006 using the methods described by *Nikolaidis* [2002]. In summary, the noise in these data has been reduced by estimating and removing a common mode signal from each time series using the algorithm of *Wdowinski et al.* [1997]. Eight GPS sites are used as fiducial sites within the region (Figure 1); and the rate of displacement, the amplitude and phase of an annual and semi-annual sinusoid, and offsets, plus any exponential decay due to postseismic slip, are estimated for each component (north, east, and up) for these sites. The stack of residual time series for each component is averaged and identified as the common-mode signal. The common-mode signal for each component is subtracted from all of the time series of position changes within the regional network.

[10] I further restrict my analysis to sites with more than 3.9 years of observations since 1996, when SCIGN started. Although many sites have data that predated 1996.0, I chose not to use them because the analysis of *Williams et al.* [2004, Figure 7] showed that the precision of data prior to 1996 is lower than current standards. In addition, not analyzed is data from sites where not analyzed is data from sites where there were significant gaps in the time series, or significant problems with the receiver, or localized environment which contributed to greater scatter in the time series. In total, time series data from 236 sites are examined. The median time span is 6.5 years, with half of the data spanning the interval between 5.3 and 7.1 years. The minimum number of observations for any of the time series is 970 points spanning 3.9 years. In contrast, the *Williams et al.* [2004] analysis of the regional SCIGN and BARGEN networks used time series, that, on average, span 3.2 years, which is well below the cut-off used here.

Table 1. Categories of Monument Types

Abbreviation	Number	Description
B+	26	BARGEN network only; deeply braced monuments
Bp		SCIGN sites identified by *Bawden et al.* [2001][a] as having man-made deformation
B1	13	originally Bp type but with RMS Seasonal >2.5 mm
B3	19	originally Bp type but with RMS Seasonal <2.5 mm
B	127	SCIGN sites using deeply braced monuments but are not Bp
B−	13	SCIGN sites using braced monuments but are not drilled to depth; Many of these are installed in rock outcrops
B2	6	originally B or B− but with RMS Seasonal >2.5 mm
P	14	rock pin; a single pin installed into a rock outcrop
R	10	GPS antenna installed on a roof of a building
C	4	GPS antenna installed on a cement platform
0	4	GPS antenna installed on a tower, dam, or oil platform

[a]See http://quake.wr.usgs.gov/research/deformation/modeling/socal/la/index.html.

[11] Prior to analyzing these data, each time series was visually examined to detect offsets, from both earthquakes and man-made causes, gross outliers due to malfunctioning equipment, postseismic deformation, and other signals that might not be tectonic in origin. Many of the time series had been edited by SOPAC to delete outliers so the time series were relatively clean. Although SOPAC provides estimates of rates, offsets, annual and semi-annual trends, and postseismic functions, these were not used here. Rather, times of offsets were tabulated. Gross outliers were deleted. For most sites located near the 1999 M7.1 Hector Mine earthquake, other functions were tested to characterized postseismic deformation, including logarithmic, exponential, or rate change. In most cases, in contrast to *Nikolaidis* [2002], I found that the logarithmic Omori's Law best characterized the postseismic deformation. Postseismic deformation was not considered from either the 2003 San Simeon or the 2004 Parkfield earthquakes since the boundary of the study area was drawn to exclude that part of Central California. Finally, several sites exhibited large deformations in response to likely recharge of local aquifers from heavy, winter rainfall [*King et al.*, 2007]. Since this event occurred in late 2004 and early 2005, the observations were deleted at those sites after late 2004.

[12] Along with analyzing the time series for noise content, the log sheets, and when available, photographs of each site were examined to determine the type of monument used. In addition, other factors were noted which might contribute to higher noise than the norm. The relationship of each site to anthropogenic sources of deformation identified by *Bawden et al.* [2001] and http://quake.wr.usgs.gov/research/deformation/modeling/socal/la was noted. On the basis of the information on hand, I put each site under one of the eight different categories of monuments listed in Table 1.

[13] Analysis for the noise content of each time series was carried out using the maximum likelihood estimator (MLE) described by *Langbein* [2004] and available at ftp://ehzftp.wr.usgs.gov/langbein/est_noise. Along with the parameters that describe a temporal function that includes rate, offsets, annual and semi-annual sinusoids, and postseismic terms, the amplitudes of the noise parameters of the assumed noise model were simultaneously estimated. Six different noise models were tested, which were flicker noise (FL), random-walk noise (RW), power law noise (PL), a combination of flicker and random-walk noise (FLRW), a combination of first-order Gauss-Markov plus random-walk noise (FOGMRW), and a combination of bandpass filtered and power law noise(BPPL). In all of these models, the amplitude of white noise was estimated, too.

[14] Both FL and RW noise models should be considered as the null hypothesis since both of these noise models are the simplest, having only two parameters: the amplitude of white noise and the amplitude of either the flicker or random-walk component. Of the two models, the better model was identified as the one with the larger MLE (actually, the maximum logarithm of the likelihood function). The addition of PL noise includes an additional parameter that is estimated, which is the power law index.

[15] BPPL noise is used here on the basis of *Langbein* [2004], who found that approximately 30% of the EDM baselines had components of seasonal noise that were smeared over a frequency band centered at 1 cycle per year. The pass band for the filter is chosen to lie between 0.5 and 2 cycles per year. The sharpness of the filter is adjusted by the number of poles used to construct the filter. The bandpass filter noise augments the annual and semi-annual terms used in the function that describes the temporal character of the data.

[16] The combination of flicker and random-walk noise (FLRW) is an attempt to categorize two different mechanisms that could contribute to the temporal covariance in GPS data. The random-walk noise characterizes the localized random motions of the monument and dominates the noise at the lowest frequencies. Flicker noise, on the other hand, characterizes the process that might be tied to the GPS system and dominates the frequency band between the high frequencies, or white noise component, and the lowest frequencies, the random-walk component. The noise from the GPS system might come from many sources, including unmodeled tropospheric delays and unmodeled components of the satellite ephemeris. In many cases, the PL noise, where the index is between 1 and 2, might be a manifestation of the FLRW noise.

[17] The FOGMRW noise is similar to the FLRW and PL noise where for the frequency band between the white noise and the random-walk noise, the spectrum is that of first-order Gauss-Markov noise. For these middle frequencies FOGM noise attempts to mimic the flicker portion of the spectrum. Thus in this case, the FOGM noise component can be thought of as a contribution by the GPS system; the random walk could be due to the monument noise. In addition, since both RW and FOGM noise models can be written as simple differential equations, the use of FOGMRW noise in Kalman filter algorithms [e.g., *Segall and Matthews*, 1997] that invert GPS data for temporal

Table 2. Median and Inter-Quartile Range for Estimates of White and Flicker Noise; Comparison of Results From *Williams et al.* [2004] and This Report

	White Noise, mm			Flicker Noise, $(mm/a)^{0.25}$				
Analysis	North	East	Vertical	North	East	Vertical	Sites Used	$T_{ave.}$ Years
SCIGN								
Williams et al. [2004]	0.7 ± 0.2	0.8 ± 0.3	3.0 ± 0.6	1.9 ± 1.1	1.9 ± 1.3	5.8 ± 3.7	147	2.7
This report	0.5 ± 0.2	0.6 ± 0.2	2.3 ± 0.5	1.3 ± 0.8	1.5 ± 0.7	4.6 ± 1.3	210	6.7
BARGEN								
Williams et al. [2004]	0.5 ± 0.1	0.7 ± 0.2	2.2 ± 0.5	1.2 ± 0.4	1.2 ± 0.7	5.4 ± 3.1	47	4.7
This report	0.6 ± 0.1	0.7 ± 0.2	2.3 ± 0.3	0.8 ± 0.3	0.9 ± 0.2	3.6 ± 1.1	26	6.8

variations in fault slip or dike intrusions could be implemented over their assumed RW models.

3. Results

3.1. Comparison With *Williams et al.* [2004]

[18] Tables 2 and 3 summarize the comparison between this paper and that of *Williams et al.* [2004], estimating the parameters for FL and PL noise models. As was done here, *Williams et al.* [2004] examined both SCIGN and BARGEN data using the SOPAC processing that included improved precision by removing the common-mode components [*Nikolaidis*, 2002]. For the SCIGN data, the results shown in Table 2 indicate that the amplitudes for both white noise and flicker noise estimated here are less than those obtained by *Williams et al.* [2004]. For the BARGEN data, the estimates of white-noise amplitudes from both reports are similar, but I found slightly lower amplitudes for flicker noise. There are several causes that might contribute to the differences, including the actual GPS sites included in the analysis, criteria for rejecting outliers, offsets detected and modeled, and the function used to model postseismic deformation.

[19] However, the comparison of results shown in Table 3 indicates that the estimates of power law index for the SCIGN data are, on average, smaller for the analysis by *Williams et al.* [2004] than I found. For the BARGEN data, the indices are, on average, equivalent. Reasons for the differences are the same as mentioned above.

[20] Nonetheless, the estimates of the flicker noise amplitudes obtained by me indicate that I have examined data that were as clean, if not cleaner, than those analyzed by *Williams et al.* [2004].

3.2. Best Noise Models

[21] Using the methods described by *Langbein* [2004], the best noise model among the six models is selected for each time series on the basis of the value of the MLE coefficient. For any time series, the MLE coefficient will be larger with the noise models having more parameters. However, tests by *Langbein* [2004] provide a conservative basis to either accept or reject the more complex model over the simpler model. Initially, the null model of either RW or FL noise is selected on the basis of the one with the larger MLE. Next, the values of MLEs from the PL and FLRW noise models are compared with those from the null model; if either of these more complex models (each having three parameters rather than the two parameters for the null model) has MLEs exceeding 2.6 units [*Langbein*, 2004] over those from the null model, then that model is considered to be better. If both the PL and FLRW models provide significant improvement in fit, then the model having the larger MLE is selected as best. Likewise, the MLEs from BPPL and the FOGMRW models are compared with the so-called best model using the same 2.6 units threshold with the exception for FOGMRW noise, where the threshold is increased to 5.2 following the results of *Langbein* [2004, Figure 4].

[22] Table 4 provides the distribution of the optimal noise models for the combined SBAR and SCIGN data. Roughly 50% to 60% of best noise models are either FL or RW noise. The combination of FL and RW or PL noise characterizes between 25% and 30% of the time series; the remaining 15% of the time series are split between the most complex noise models: BPPL and FOGMRW.

Table 3. Power law Indices; Comparison of Results From *Williams et al.* [2004] and This Report

	Power Law Index; Mean and Stan. Dev.	
Component	*Williams et al.* [2004]	This report
SCIGN		
North	1.1 ± 0.5	1.4 ± 0.5
East	1.1 ± 0.6	1.5 ± 0.4
Vertical	0.9 ± 0.5	1.4 ± 0.4
BARGEN		
North	1.4 ± 0.4	1.0 ± 0.5
East	1.0 ± 0.4	1.1 ± 0.4
Vertical	0.9 ± 0.4	1.0 ± 0.3

3.3. FLRW and FOGMRW Noise Versus PL Noise

[23] The suitability of the combination of FL and RW (or FLRW) noise model versus the PL noise model is explored in Figure 2a, where the differences in MLE between the FLRW and PL noise models are plotted versus the estimated PL index. I wish to test the possibility that for those time series where the power law index is between 1 and 2, a combination of flicker and random-walk noise is a viable alternative noise model. If the difference in MLEs between FLRW and PL noise is less than zero, then the PL noise would be the better choice of model. The results show that, for PL indices that are either less than 1 or greater than 2, the

Table 4. Best Noise Model for SCIGN and SBAR Data

	Percentage of All Sites		
Noise Model	North	East	Vertical
FL	32	27	41
RW	21	35	18
PL	11	11	6
FLRW	20	16	21
FOGMRW	8	3	9
BPPL	8	9	5

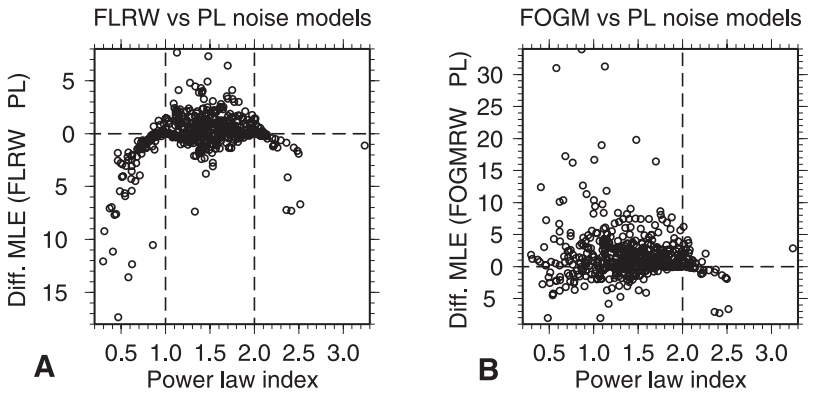

Figure 2. Plots of the difference in logarithm of MLE versus power law (PL) index. In Figure 2a, the differences of MLE between FLRW and PL noise models are shown. A positive difference indicates that FLRW is a better model than PL. In Figure 2b, the differences of MLE between FOGMRW and PL noise are shown. A positive difference does not necessarily indicate the FOGMRW model is better than the PL model. See text.

differences in MLEs are less than zero, indicating the PL noise is the better of the two models. For indices that are close to either 1 or 2, the MLEs are nearly zero, indicating that the noise process is either flicker or random walk. However, for indices that are between 1 and 2, the MLEs, on average, tend to be positive, suggesting that the FLRW noise model better matches the data, which is also suggested in Table 4 comparing the best noise model type between PL and FLRW noise.

[24] The suitability of FOGMRW noise relative to PL noise is shown in Figure 2b. In this comparison, the value of MLE for the FOGMRW noise model generally exceeds the MLE for the PL noise model. This is understandable since there are three parameters that describe the FOGMRW model versus the two that describe the PL model. Unlike the relationship shown in Figure 2a with the FLRW model, the difference between FOGMRW and PL appears to be independent of the PL index.

3.4. Common-Mode Seasonal Noise

[25] *Bawden et al.* [2001] showed that many of the GPS sites in SCIGN had large, annual signals because these sites are located within or near areas of active groundwater or oil pumping. They used a combination of InSAR images of deformation and time series of GPS data to make their comparison. Many of the images from InSAR showed large, near vertical deformation in areas where there is known pumping. These images of deformation, especially those

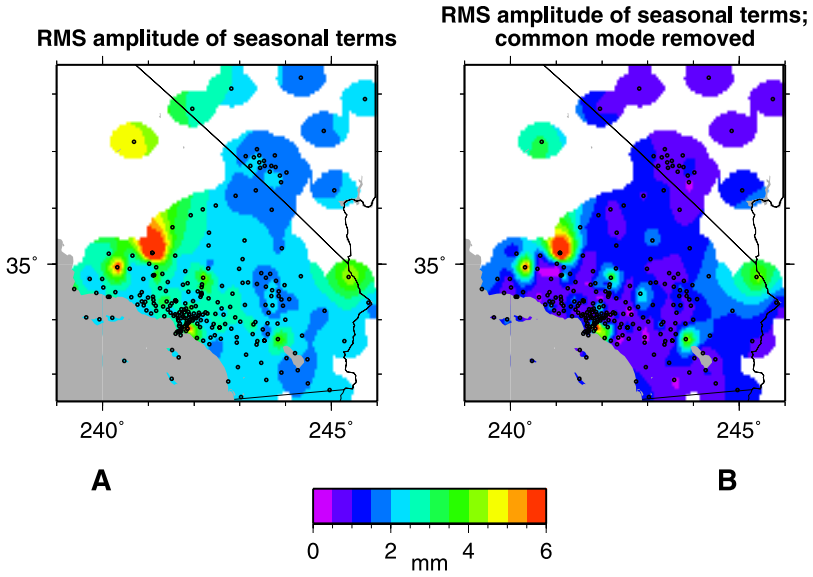

Figure 3. Map showing the distribution of the amplitude of seasonal deformation for both the SCIGN and SBAR sites. Laplacian smoothing of the seasonal amplitudes was done prior to plotting. In Figure 3a, these amplitudes are extracted from fits of annual and semi-annual sinusoids to the time series of GPS displacements. The magnitudes of the sinusoids have been combined as described in the text. In Figure 3b the magnitudes of seasonal displacements are shown after removing the common-mode annual and semi-annual seasonal displacements.

Table 5. Common-Mode Annual and Semi-Annual Terms[a]

	Amplitude, mm			
	One-Year Period		One-Half Year Period	
Component	$\cos(2\pi t)$	$\sin(2\pi t)$	$\cos(\pi t)$	$\sin(\pi t)$
North	0.37	0.73	−0.22	−0.26
East	0.34	−0.37	−1.08	−0.17
Vertical	1.41	−1.87	−0.09	−1.34

[a]Relative to 1 January, time, t, in years.

that span a half-cycle of annual pumping used to fill local aquifers for water storage, provide the spatial distribution of deformation due to pumping. For GPS sites located within the area of active pumping, the deformation due to the recharge is predominantly vertical. However, for GPS sites located near, but not on top of, active pumping, the deformation can be nearly horizontal.

[26] *Bawden et al.* [2001] limited their search of InSAR images to the immediate area around Los Angeles, where many of the SCIGN stations were located at the time of their report. However, now, the number of SCIGN sites has nearly doubled and many of the newer sites are located away from the immediate Los Angeles area. Consequently, it might be useful to use the estimates of amplitude of the annual periodicity from the GPS data analyzed here to locate additional areas that might be affected by nearby pumping and for which there are no known InSAR studies. In doing this study, I can compare the seasonal amplitudes of all of the GPS sites shown in Figure 1 with those amplitudes of the sites identified by *Bawden et al.* [2001] as being affected by anthropogenic sources or, in the terms of monuments listed in Table 1, as Bp.

[27] Both the annual and semi-annual terms for each component are combined into a single term defined by $(A^2_{e365} + A^2_{e182} + A^2_{n365} + A^2_{n182} + A^2_{u365} + A^2_{u182})^{0.5}$ where A_{xD}, is the amplitude of the x component with a period of D days (Figure 3a). Although the direction and phase of the annual deformation are lost in this parameterization, there is one feature that is significant: all sites have at least 2 mm of seasonal deformation. This suggests that the annual deformation could have a common source.

[28] To test the hypothesis of a common-mode signal, the amplitude and phases of the annual and semi-annual terms of deformation for each component of each site were tabulated. Then, for both the annual and semi-annual periods, I determined the median amplitude and phase across all sites (Table 5), whose time series is shown in Figure 4a, and removed that common mode periodicity for the time series of each site.

[29] The residual amplitude of seasonal noise (Figure 3b) indicates that most of the GPS sites have residual amplitudes less than 1 mm. Large amplitudes, greater than 2.5 mm, are restricted to a few areas, such as the Los Angeles basin, or a few isolated sites.

[30] Of the 236 sites that I analyzed, 32 of the sites were identified by *Bawden et al.* [2001] as being influenced by nearby pumping. Of those 32 sites, I determined that 13 of them have seasonal amplitudes greater than 2.5 mm. In addition, I have determined that there are 6 sites that have braced monuments, with more than 2.5 mm of seasonal deformation, but were not identified by *Bawden et al.* [2001] as problematic sites. Many of those sites were not analyzed by *Bawden et al.* [2001] because of the reasons discussed above. For these 6 sites, Bawden [personal communication 2006] has recently examined InSAR interferograms and determined that two sites are near areas of active pumping and should be affected, and three others might be affected by active pumping. The high seasonal signal for the remaining site, NDAP, at Needles Airport, near the point where borders of the states California, Nevada, and Arizona converge (Figures 1 and 3b), remains unexplained since the existing InSAR interferograms do not indicate any seasonal deformation. Since it might be possible that seasonal behavior could be affecting the long-term stability of braced monuments, three additional designations of monument types, B1, B2, and B3, are added to Table 1.

3.5. Ranking of Monument Types

[31] *Williams et al.* [2004] used Wilcoxon paired ranking to show that deeply braced monuments used in the SCIGN network had less noise than other types of geodetic monument. They used two different metrics of time series noise to rank their data; for the analysis presented here, I believe there is a better metric. The two metrics employed by *Williams et al.* [2004] are the time required for the estimate

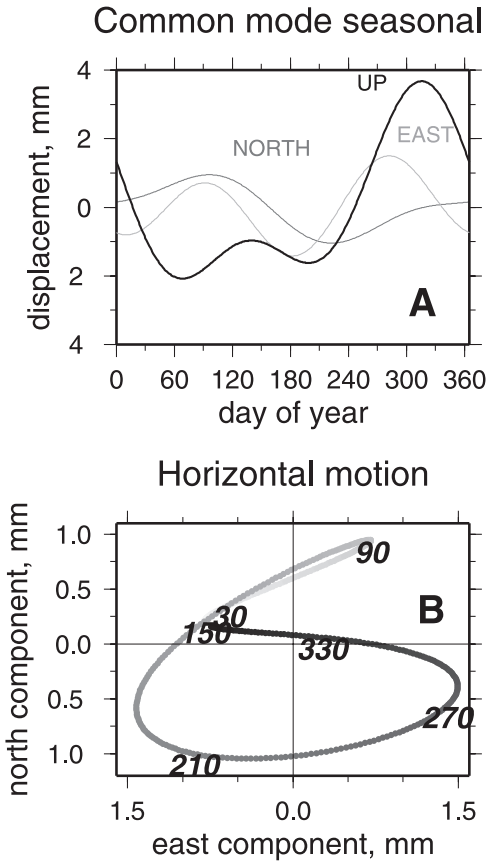

Figure 4. Seasonal common-mode deformation for the combination of SCIGN and SBAR sites. In Figure 4a, the median annual and semi-annual displacement for north, east, and up are shown for a one-year period starting on 1 January. In Figure 4b the median horizontal displacement is replotted in terms of eastward and northward drift. The day of the year is shown as a gray scale and called out every 60 days.

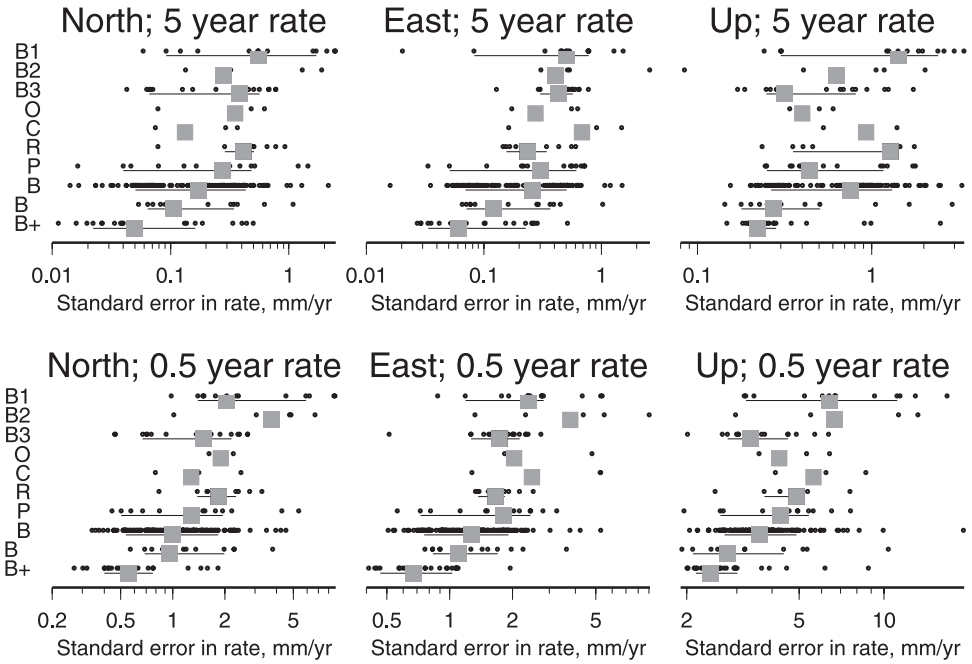

Figure 5. Scatterplot showing monument type versus the standard errors in rates estimated for 5 years and a rate change lasting 0.5 years using the best noise model for each time series of displacements. The dots are the estimates of standard error, the large gray square is the median of the standard error for each monument type, and the gray line shows the interquartile range of the estimates. See Table 1 for the description of monument types.

of standard error in rate to be less than 1 mm/a and the amplitude of random-walk noise. Since many data sets are not well represented by random-walk noise, ranking monument types by that metric is not appropriate. In addition, although time required to achieve a desired level of standard error in rate is a reasonable metric, this metric only gives one measure of the noise spectra. Instead, I propose that the standard errors in rate estimated for 0.5 and 5 year time spans are better metrics to rank the monument types; one metric samples the noise at periods where monuments tend to have seasonal fluctuations and the second samples the noise at longer periods that are used to determine site velocities of tectonic motion. These metrics encompass the possibility that the noise spectra representing the data can be made up of a combination of noise models; some of the components impact the data at periods of less than one year and other components of the model impact those data at longer periods.

[32] For each component at each site, the best noise model previously identified is used to construct a data covariance matrix for a 5.5 yearlong time series that has no gaps. A time-dependent model of a constant rate for the first 5 years and a rate change for the last half year is used; from that model and the data covariance, the standard error in rates for 5 and 0.5 years are determined and recorded. Thus each component at each site has two metrics that are based upon the noise model associated with the original data: one associated with its long−term rate and a second metric that measures the sensitivity to rate changes.

[33] The estimated standard errors in rate and rate changes for each time series versus the monument types (Figure 5) range from 0.01 to 2 mm/a for the standard error of rates in the horizontal displacements over 5 years; likewise, the range is from 0.3 to 8 mm/a for rate change over 0.5 years. However, there are some systematic trends. Examination of the median value (Figure 5) suggests that both the B+ and B− monument types yield smaller standard errors than B1, B2, and B3 monuments. That is, the monuments identified as B+, which comprise the SBAR network, and B-, most of which are short-braced monuments installed in rock, tend to provide the best precision. Conversely, the braced monuments that are near active pumping (B1 and B3) or have large seasonal amplitudes provide the lowest precision. Of course, these generalizations need to account for the spread of the results shown in Figure 5.

[34] The generalizations relating monument type and precision can be tested using the Wilcoxon rank sum test [e.g., *Wilcoxon*, 1945]. Results of pairing monument types are shown in Table 6, where the distribution of standard errors for each monument type are compared. Those pairings in bold print represent the statistical confidence that the first monument type yields better (or less) precision than the second type at the $\leq$1% (or $\geq$99%) confidence level. For pairings in italics, the level of significance ($\leq$5% or $\geq$95%) is interesting but not overwhelming. From this test, it is clear that the B+ or SBAR monuments yield the best precision. Also, the B1 monuments, that is, those monuments that are near active pumping and have a large seasonal response, yield the worst precision when compared to the standard, deeply braced monuments (B) or short-braced monuments (B-). For the other pairings, the superiority of one monument against another is not strongly significant ($\geq$99%).

Table 6. Pairwise Ranking of Monument Types

Monument Pair		Long Term Test			Short Term Test		
		N	E	U	N	E	U
B+	B1	**0.0**	**0.0**	**0.0**	**0.0**	**0.0**	**0.0**
B+	B2	**0.1**	**0.0**	*2.0*	**0.0**	**0.0**	**0.0**
B+	B3	**0.0**	**0.0**	**0.1**	**0.0**	**0.0**	**0.1**
B+	B−	**0.1**	**0.2**	7.0	**0.0**	**0.0**	8.7
B+	B	**0.0**	**0.0**	**0.0**	**0.0**	**0.0**	**0.0**
B+	C	*3.5*	**0.1**	**0.2**	**0.4**	**0.0**	**0.1**
B+	P	**0.6**	**0.1**	**0.0**	**0.1**	**0.0**	**0.0**
B+	O	**0.6**	**0.3**	**0.9**	**0.0**	**0.0**	**0.6**
B+	R	**0.0**	**0.0**	**0.0**	**0.0**	**0.0**	**0.0**
B1	B2	71.1	68.9	94.6	29.4	12.1	48.1
B1	B3	*96.2*	83.8	**99.9**	**99.2**	**99.5**	**100.0**
B1	B−	**99.2**	**99.7**	**99.8**	**99.9**	**99.9**	**100.0**
B1	B	**100.0**	**100.0**	**99.9**	**100.0**	**100.0**	**100.0**
B1	C	*95.2*	23.9	92.1	96.2	31.0	76.0
B1	P	*98.2*	89.6	*98.7*	**99.3**	*97.7*	**99.3**
B1	O	85.5	76.8	94.7	76.2	68.6	88.1
B1	R	82.9	*97.5*	92.6	86.1	**99.0**	*98.1*
B2	B3	76.5	46.8	83.4	**99.9**	**99.4**	**99.5**
B2	B−	*95.0*	**99.4**	87.5	**99.8**	**99.9**	**99.8**
B2	B	*96.5*	**99.7**	65.8	**100.0**	**100.0**	**99.8**
B2	C	87.0	30.3	46.1	*98.2*	69.5	76.6
B2	P	84.1	77.7	69.6	*98.9*	**99.2**	**99.0**
B2	O	53.4	69.6	91.6	*96.8*	87.1	94.7
B2	R	31.7	*96.2*	32.5	**99.0**	*98.6*	*97.5*
B3	B−	88.3	**99.9**	84.6	64.6	*98.7*	91.1
B3	B	*98.5*	**100.0**	*4.5*	*97.0*	**100.0**	28.6
B3	C	81.2	6.7	5.6	51.7	*4.9*	**0.7**
B3	P	71.5	78.5	15.5	65.2	49.9	*4.7*
B3	O	42.7	74.2	41.6	11.8	8.2	*2.5*
B3	R	11.4	*98.8*	*1.7*	5.9	78.1	**0.7**
B−	B	63.0	27.4	*1.6*	85.7	61.4	5.5
B−	C	38.6	*2.3*	5.2	26.8	*1.5*	*1.3*
B−	P	33.5	9.4	*4.6*	47.7	15.0	6.2
B−	O	17.6	9.9	17.6	9.9	*1.4*	*5.2*
B−	R	*1.2*	13.2	*2.7*	*2.7*	5.8	*3.4*
B	C	37.3	*1.2*	15.7	12.3	**0.4**	**0.2**
B	P	20.9	6.3	53.5	11.3	*1.4*	*2.2*
B	O	6.8	9.9	86.8	**0.4**	**0.1**	*3.2*
B	R	**0.0**	23.9	7.0	**0.0**	**0.1**	**0.2**
C	P	36.3	94.5	83.5	56.3	*95.9*	*95.1*
C	O	17.9	90.2	*98.7*	17.1	83.3	83.0
C	R	*2.0*	96.0	52.4	11.6	90.5	92.4
P	O	25.9	47.7	70.4	7.3	13.7	40.0
P	R	6.8	79.3	13.3	5.3	60.1	30.9
O	R	24.6	84.9	11.9	57.8	97.5	52.9

3.6. Spatial Distribution of Noise

[35] The mapping of the distribution of the standard errors in rate shows some spatial coherence of the data for the SCIGN and SBAR networks (Figure 6). Included are those monuments grouped to be B+, B, B−, and Bp but with seasonal noise less than 2.5 mm (B3).

[36] One possibility to test is the effect of rainfall on the standard error in rates. Average annual rainfall values were obtained for nearly 1000 sites distributed in California and Nevada from the National Climatic Data Center and recompiled by the Desert Research Institute (J. Ashby, personal communication, 2007). Sites were selected that had more than 20 years of observations and have had measurements since 1995. About 200 sites distributed across the Southern California and Nevada regions were found suitable. From those rainfall data, an over-sampled set of rainfall data was created by interpolating the original data set on a 0.05° by 0.05° grid. Then, from the site location of each GPS receiver, the average annual rainfall at that site could be estimated. A plot of standard error in rate versus the annual rainfall is shown in Figure 7. A log linear trend relating rainfall to logarithm of standard error in rate, $\log(E) = E_o + \alpha R$, is also plotted for each component of GPS, where R in cm/a is rainfall, and E in mm/a is the standard error in rate. The logarithm of the standard error in rate, rather than simply the standard error was chosen for the convenience of plotting. A L1 norm was used to fit these data and, for the three comparisons, the value of the rainfall dependence, α, is non-zero.

[37] Since it is clear that the distribution of standard errors in rates is not normally distributed about the linear trends shown in Figure 7, I used bootstrap analysis [e.g., *Efron and Tibshirani*, 1993] to estimate whether the value of the slope, α is non-zero. For each of the three fits shown in Figure 7, this involved 1000 re-samples of the data and estimates the linear fit after creating a new population. From the distribution of the estimates of α, the significance of the slope was determined (Table 7). The results suggest that the north standard error in rate has a rainfall dependence with a 99% confidence level, but the east and vertical components have a weak dependence, rated with 67% and 90% confidence level respectively.

4. Discussion

[38] In this report I have applied techniques of noise modeling developed by *Langbein* [2004] for EDM data to GPS time series data and secondly, examined in more detail

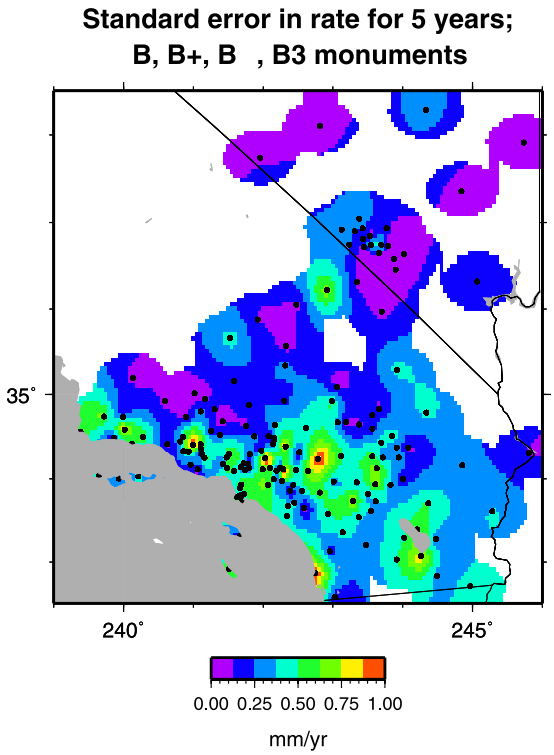

Figure 6. Map showing the distribution of standard error in 5 year rates for SCIGN and SBAR networks using the best noise model for each time series. Included are only braced monuments that have seasonal amplitudes of less than 2.5 mm. Sites with standard errors in excess of 1 mm/a are colored as if they are 1 mm/a.

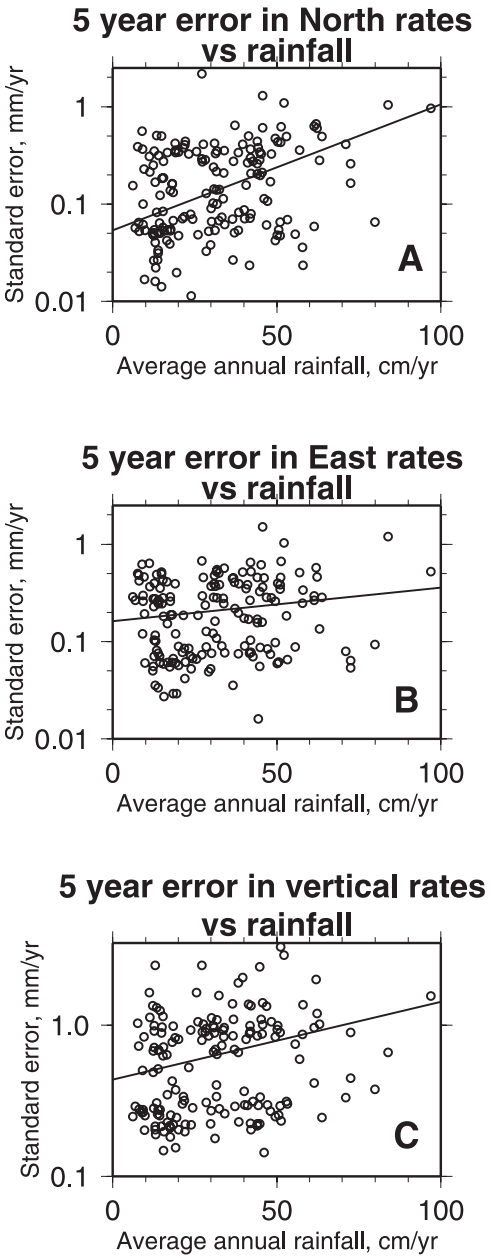

Figure 7. Standard error in 5-year rates for east, north and vertical components plotted against average, annual rainfall recorded near the GPS sites. Included are only braced monuments that have seasonal amplitudes of less than 2.5 mm. In Figure 7a, the circles are the standard errors in the north component. The solid line is the best fit trend between the north and the precipitation data. Likewise, Figure 7b shows the east component and Figure 7c shows the vertical component.

the monument stability problem for GPS that was explored by *Williams et al.* [2004]. Along the way, I have also uncovered a seasonal, common-mode signal present in SCIGN and SBAR data that is present in the SOPAC processing of GPS data where spatial filtering [*Wdowinski et al.*, 1997; *Nikolaidis*, 2002] was used. The results of my analysis of the noise models for this limited set of GPS time series of position changes have some implications which I will discuss below.

[39] The noise modeling of GPS data by *Williams et al.* [2004] only included power law noise; the power law includes both flicker and random-walk processes. However, *Langbein* [2004] found that the EDM data required more complex noise models which for many time series required stochastic, seasonal noise that is termed ''band-passed filtered'' (BP) noise. Of the 39 baselines analyzed by *Langbein* [2004], he found that 40% contained BP noise in their time series. However, the results of my analysis of GPS data contained here indicate that only a low percentage, between 5 and 9% of the sites, required a BP component (Table 4). In addition, an equally small percentage of GPS time series had a FOGM component in their noise spectra. Also, if I count the flicker plus random-walk noise model to be nearly equivalent to a power law process with an index between 1 and 2, then the PL process proposed by *Williams et al.* [2004] for GPS data is consistent with the results presented here.

[40] On the other hand, the results presented in Figure 2a suggest that the power law model of noise may actually be a combination of two noise processes, flicker and random walk. For application of the maximum-likelihood algorithm that I have used to find the optimal noise model, the combination of flicker and random walk is somewhat less CPU intensive than the power law noise model. Both models have two unknowns: PL has the index and its amplitude, and FLRW has amplitudes for both components. In constructing the PL covariance, this requires evaluation of equation (9) of *Langbein* [2004] at each iteration. In contrast, the FLRW, equation (9) of *Langbein* [2004] need only be evaluated once for flicker and once for random walk and simply stored in the computer's memory; only the amplitude needs to be varied. Using the PL model rather than the FLRW model increases the computation time by approximately 50%.

[41] More importantly, the concept of a noise model consisting of a combination of two processes, flicker and random walk, is physically more attractive than simply a power law process. Arguably, one could consider that the flicker noise is a result of the GPS system exclusive of the monument and the random-walk component is a result of random motions of the monument. By the GPS system, I include the GPS receiver, the satellites, the models used to process the GPS observables, and the local environment of the antenna. In other studies of noise from surface and near-surface instruments, namely strainmeters [*Wyatt*, 1982; *Wyatt*, 1989; *Agnew*, 1992; *Johnston and Linde*, 2002] and creepmeters [*Langbein et al.*, 1993], the spectra from

Table 7. Dependence of 5-Year Standard Error in Rate With Average, Annual Rainfall

GPS Component	α[a] log (mm)/cm	Confidence Level	Confidence Interval Log (mm)/cm
East	0.0034	67%	−0.0003 to 0.0063
North	0.0130	99%	0.0013 to 0.0187
Combined			
East and North	0.0037	90%	0.0003 to 0.0075
Vertical	0.0051	90%	0.0000 to 0.0100

[a]Slope of fit of standard error in rate to rainfall, Figure 7.

Table 8. Nominal Values for Flicker and Random-Walk Model of Noise

Parameter	Units	Median	Inter-Quartile Range
North			
White noise	mm	0.55	0.44 0.76
Flicker noise	mm/a$^{0.25}$	0.9	0.4 1.6
Random-walk noise	mm/a$^{0.5}$	0.5	0.0 1.4
East			
White noise	mm	0.67	0.55 0.86
Flicker noise	mm/a$^{0.25}$	0.9	0.3 1.6
Random-walk noise	mm/a$^{0.5}$	0.7	0.0 1.4
Up			
White noise	mm	2.36	2.02 2.90
Flicker noise	mm/a$^{0.25}$	3.6	2.3 5.9
Random-walk noise	mm/a$^{0.5}$	1.5	0.0 2.9

the data are close to those from a random walk. *Langbein and Johnson* [1997] argue that noise from monuments used in EDM should be close to random walk, too. *Langbein* [2004, Figure 8a] essentially confirmed that notion, where he found that the indices of the power law clustered close to 2.0, or that of random walk.

[42] Another attractive feature of the FLRW model over the PL model is that it can provide users of GPS time series data guidelines of nominal levels of noise to use with these data. The preference for the FLRW model over the PL model is the unambiguous specification of its amplitudes. In PL noise, the specified amplitude is closely tied to the power law index, as revealed by *Williams* [2003, equation (10)]. As an example, for two different power laws, one with an index of 1.5 and a second with 1.6, which have the same power at 1 cycle/a, the amplitude needed to specify the covariance matrix differs by 5% with a 0.1 change in index. With FLRW, there is no trade-off between the specified amplitudes; this feature is exploited in Table 8 to give nominal coefficients that characterize the GPS data covariance estimated from all of the time series examined here. For instances where one does not desire to estimate the optimal noise model for each GPS time series individually with an MLE code [ftp://ehzftp.wr.usgs.gov/langbein/est_noise or http://www.pol.ac.uk/home/staff/?user=WillSimoCats], the values listed in Table 8 could be plugged into these codes without doing the optimization. Using 0.7 mm for white, 1.0 mm/a$^{0.25}$ for flicker, and 1.0 mm/a$^{0.5}$ for random-walk should provide conservative estimates of the standard error when fitting various functions of time to time series of horizontal position changes derived from regionally filtered GPS data. Inspection of the time series and judgment will allow one to choose different values for the noise model. For instance, benchmarks often used in campaign GPS surveys could be considered less stable than the ones evaluated here, for which one might want to double the recommended noise parameters. On the other hand, I found that more one-half of the time series for B+ monuments had no detectable, random-walk noise. Thus for the sites in the SBAR network, one could use values less than 0.5 mm/a$^{0.5}$ in modeling the noise of these data; flicker and white noise for B+ are equivalent with those in Table 8.

[43] In this report, I have examined the FOGMRW noise, not because I believe it is necessarily an accurate description of the stochastic processes in the GPS system, but because it could be used in the Kalman Filter schemes [e.g., *Segall and Matthews*, 1997] used to extract temporally and spatially coherent tectonic signals from GPS data. The Kalman filter requires that the noise process can be written with a finite number of coefficients. The general power law relation requires an infinite number of terms. In the current implementation of Kalman filter schemes for inverting GPS data, only white noise and random-walk noise models are considered since these can be written simply. However, the combination of these two models only represents a small fraction of GPS data. Most GPS data have a power law index between 1 and 2. To mimic that behavior and still meet the requirements needed to be included in Kalman filters, the combination of FOGM and RW noise is tested here as a substitute for PL noise. In Figure 2b, for many cases the FOGMRW noise provides a satisfactory representation of GPS noise; much better than had only RW been employed. I would recommend using FOGMRW noise in Kalman filter techniques used to model GPS measurements as the FOGM component can also be written in terms of a few coefficients.

[44] Examination of Figure 3a for seasonal noise is indeed discouraging since the minimum amplitude is 2 mm. Testing of braced monuments located in Central California by *Langbein et al.* [1995] at sites with known seasonal noise indicated that these monuments are effective in reducing the amplitude of this periodic noise. I would have expected sites located in the drier areas Southern California and Nevada relative to those in Central California to have seasonal signals that were much less than 2 mm. With the uncovering of the seasonal signal that is common to all sites (Figure 4a and Table 4), the picture shown in Figure 3b indicates that many sites had seasonal amplitudes less than 0.5 mm. The time series of the common-mode seasonal signal in Figure 4b suggests that in January of each year, the GPS network as a whole displaces west by 1 mm; by April it displaces to the northeast, then by June it returns to its April position. Through the summer and fall, the network displacements rotate from the west through the south and then east; by early December the amplitude of the displacement is zero, but during that month the network rapidly displaces to the west. While the network is displacing to the east in the late fall, it is simultaneously uplifted by 4 mm (Figure 4a). A rapid subsidence follows during the winter.

[45] *Dong et al.* [2002] analyzed many sites in the global GPS network in terms of seasonal displacements. In particular, they found that the vertical displacements exceeded the horizontal, which is confirmed in this study, too. In addition, for the Southern California region, they found that the vertical displacement was approximately 5 sin ($2\pi t$-π) mm, where t is the time in years relative to 1996.0. This indicates that the maximum subsidence occurs in March and the maximum uplift occurs in September of each year. My estimates of phase of annual vertical motion, shown in Figure 4a, agree with those from *Dong et al.* [2002]; however, my amplitude for the annual term is 2.5 mm, which is about 50% of the estimate provided by *Dong et al.* [2002, Figure 2].

[46] A common-mode seasonal signal has been noted for other GPS networks, most recently by *Bettinelli et al.* [2006] and *Ray et al.* [2006]. *Dong et al.* [2002] catalogs most, if not all, of the possible sources of seasonal variations along with further references. The list includes known, geophysical sources of the long period, polar and ocean

tides, atmospheric mass loading, non-tidal ocean loading, and snow and soil moisture loading. In addition, there are several other possible sources, which include atmospheric models, bedrock thermal expansion, phase center models of GPS antennas, GPS software, perturbations of satellite orbits, and network transformation errors. *Penna et al.* [2007] shows that aliasing of unmodeled tidal signals can leak into both semi-annual and annual periods found in GPS data.

[47] *Prawirodirdjo et al.* [2006] have also noted the common-mode, annual and semi-annual periodicity is present in SCIGN time series. However, they suggest that the cause might be thermo-elastic straining of the crust for which they present a one-dimensional model to represent the horizontal displacements. Although this can be considered a reasonable model, it too is among the list of sources presented by *Dong et al.* [2002].

[48] Given that repetitive, seasonal noise is present in the SOPAC time series of position changes, an additional step should be implemented by SOPAC to remove the seasonal signal. Prior to identifying and removing common-mode signals in GPS time series, SOPAC removes the annual and semi-annual periodic trends in each time series presumably on the assumption that the seasonal terms are site specific. Thus it is perhaps no surprise that I and others have identified a seasonal signal that is common to all sites in Southern California and Nevada. There are three methods perhaps suited to remove this common mode signal: (1) Keep the same steps already in place at SOPAC, but, as I did, retrospectively stack the seasonal terms and estimate their median amplitudes and phases and apply the common-mode to further adjust the time series. (2) When initially fitting rates, offsets, and other known functions to fit each time series prior to stacking and extracting the common-mode signal, do not include the annual and semi-annual trends. (3) Fit to the data annual, semi-annual periods, rates, offsets and other known functions, but prior to stacking, add back the annual, semi-annual trends; this minimizes the bias in estimating rate [*Blewitt and Lavallee*, 2002].

[49] Finally, the results of statistical monument intercomparison clearly indicate that the sites comprising the SBAR network provide the lowest noise. In some respects, this is not necessarily surprising as Southern Nevada has a uniformly dry climate, and the availability of rock outcrops is common throughout the region. The braced monuments installed in the SBAR network were done by a different construction firm than employed by SCIGN. However, I don't believe that differences in construction practices lead to a difference in monument performance. In the Parkfield GPS network, two of the 11 braced monuments were installed by the same firm that installed SBAR, seven monuments were installed by the same firm that installed SCIGN, and the remaining two were installed by Wyatt at UCSD [*Langbein et al.*, 1995]. Visual inspection and quantitative measures of noise of these time series [*Langbein et al.*, 2006, Table 2a in eSupplement] do not reveal a striking difference in monument performance. Rather, it is likely that the differences noted here are due to the SBAR network being located in a dry area.

[50] This paper confirms the observation made by *Williams et al.* [2004] that the sites comprising the SBAR network have the lowest noise. However, the improvement in noise performance of the braced monuments indicated by *Williams et al.* [2004] is not demonstrated here. One difference in the results presented here and that of *Williams et al.* [2004] is that I could use longer time series to examine and that differences in the long-term stability could be better resolved.

[51] Other than noting that GPS sites that comprise the SBAR network have less noise than SCIGN sites with braced monuments, Figure 6 does not reveal any striking, large-scale spatial correlation of monument noise. The results of comparing monument noise with the average, annual rainfall do show a marginally significant dependence. However, I don't believe that rainfall directly causes the monument to move randomly, but, rather rainfall contributes to weathering and erosion, which can affect the local motions of the monument. In addition, high topography or the steepness of the topography can affect the erosion rates. Decoupling topography from rainfall is difficult since high topography influences rainfall.

[52] One of the largest expenses of installing continuous GPS sites for SCIGN and SBAR was the construction of the braced monument. This cost can be more than the cost of the GPS receiver and its antenna. Thus given that the braced monument is not a clear-cut winner against other monument types listed in Table 6, it is reasonable to question whether braced monuments are worth their expense. Clearly, the best predictor of low-noise sites is location, exemplified by the SBAR network; arid climate and availability of rock for installation of monuments yield high-quality data. Unfortunately, there are other noise sources in addition to random motions of the monument that can contribute to the total noise at each site; these other sources include nearby vegetation, fences, and slightly faulty antennas. Attempting to rank the performance of different monuments becomes a nearly impossible task given the variability of settings of the sites involved in this study. Clearly, the best tests are controlled experiments where two different types of monuments are installed side-by-side, as was done by *Langbein et al.* [1995]. Even there, where both sites had large seasonal displacements and the braced monuments were clearly better attenuating the seasonal noise, the results in terms of improved long-term stability of braced monuments were ambiguous [*Langbein*, 2004]. Other controlled tests at sites where the noise is presumed to be low would be required to demonstrate the performance differences between monuments. However, given that nearly a decade of data would be required to rank monument performance, it is unrealistic to think that testing would be done prior to designing and installing a large geodetic network such as the Plate Boundary Observatory. Thus one is left with balancing the economics against what is believed to be the best monument type. Although a braced monument represents a large percentage, perhaps 40%, of the initial cost of installing a GPS site, a longer-term view suggests that the impact of the expense of the braced monument becomes less with time as one factors in annual maintenance, telemetry, and the expense of the scientist looking at the data. An upper bound of the expense of a braced monument is perhaps 25% of the total cost; this does not include the time analyzing the data.

5. Conclusions

[53] This report uses the noise models described by *Langbein* [2004] and applies them to the SBAR and SCIGN

GPS data processed by SOPAC. I have extended the initial analysis done by *Williams et al.* [2004] on many of these same time series. Differences include: (1) This report uses time series that are, on average two to three times longer than employed by *Williams et al.* [2004]. (2) I have included better models of post seismic deformation than those employed by *Williams et al.* [2004] and *Nikolaidis* [2002]. (3) This report uses other noise models than the PL model employed by *Williams et al.* [2004]. One such model, the FLRW model, which, for most GPS time series data is as good as the PL model, has one key advantage; its parameters provide a simple description of the noise properties of the data (Table 8) which can be plugged into existing software used to estimate rates, rate changes, offsets and other functions that describe the time series of deformation data.

[54] The results presented here indicate that location of the GPS site is probably the biggest predictor of its stability; sites located in the dry deserts will perform best. Sites located near areas of active pumping will perform worst. Otherwise, the design of the monument is not an obvious major factor in the overall performance in terms of correlated noise in the data presented here. If there are differences inherent to different designs in monuments, this will need further, controlled testing, where monuments of different types are installed adjacent to each other at sites that will provide the best, low-noise environment. The differences in performance will require several years of observations. In the absence of controlled testing, more studies, like this one, will be required, but using even longer time series. Presumably, if monument noise is indeed a random-walk process that is superimposed upon the flicker noise of the GPS system, then long time series will be required to accurately measure the amplitude of the random-walk noise.

[55] Finally, the time series of GPS estimates of position compiled by SOPAC contain a seasonal signal that is common to all sites. This signal can be easily removed from these time series.

[56] **Acknowledgments.** Contributions by the operators of both the SCIGN and BARGEN networks are greatly appreciated. The long-term nature of this study is dependent upon the individuals who constructed these sites and maintained the flow of high-quality data. Also, the individuals at SOPAC who wrote the code, maintained the files, and processed the GPS data are given equal credit with the network operators. Plots were made using the GMT software [*Wessel and Smith*, 1991]. Constructive reviews and comments by Jessica Murray-Moraleda, Gerald Bawden, Pedro Elosegui, Simon Williams and Duncan Agnew were used and are appreciated.

References

Agnew, D. C. (1992), The time-domain behavior of power-law noise, *Geophys. Res. Lett.*, *19*(4), 333–336.

Bawden, G. W, W. Thatcher, R. S. Stein, K. W. Hudnut, and G. Peltzer (2001), Tectonic contraction across Los Angeles after removal of groundwater pumping effects, *Nature*, *412*, 812–815.

Beavan, J. (2005), Noise properties of continuous GPS data from concrete pillar geodetic monuments in New Zealand and comparison with data from U.S. deep drilled braced monuments, *J. Geophys. Res.*, *110*, B08410, doi:10.1029/2005JB003642.

Bettinelli, P., M. Flouzat, J. Avouac, L. Bollinger, R. Cattin, and S. Sapkota (2006), Seasonal signal variations in GPS time series in the central Himalaya of Nepal, *Eos Trans. AGU*, *87*(52), Fall Meet. Suppl., Abstract G43A-0984.

Blewitt, G., and D. Lavallee (2002), Effects of annual signal on geodetic velocity, *J. Geophys. Res.*, *107*(B7), 2145, doi:10.1029/2001JB000570.

Dong, D., P. Fang, Y. Bock, M. K. Cheng, and S. Miyazaki (2002), Anatomy of apparent seasonal variations from GPS-derived site position time series, *J. Geophys. Res.*, *107*(B4), 2075, doi:10.1029/2001JB000573.

Efron, B., and R. J. Tibshirani (1993), *An Introduction to the Bootstrap: Monographs on Statistic and Applied Probability*, vol. 57, Chapman and Hall, New York.

Johnson, H. O., and D. C. Agnew (1995), Monument motion and measurements of crustal velocities, *Geophys. Res. Lett.*, *22*(21), 2905–2908.

Johnston, M. J. S., and A. T. Linde (2002), Implications of crustal strain during conventional, slow, and silent earthquakes, in *International Handbook of Earthquake Engineering and Seismology*, vol. 81A, edited by W. H. K. Lee et al., chap. 36, pp. 589–605, Int'l Assoc. Seismol. & Phys. Earth's Interior.

King, N. E., et al. (2007), Space geodetic observation of expansion of the San Gabriel valley, California, aquifer system, during heavy rainfall in winter 2004–2005, *J. Geophys. Res.*, *112*, B03409, doi:10.1029/2006JB004448.

Langbein, J. (2004), In two-color electronic distance meter measurements revisited, *J. Geophys. Res.*, *109*, B04406, doi:10.1029/2003JB002819.

Langbein, J., and H. Johnson (1997), Correlated error in geodetic time series: Implications for time-dependent deformation, *J. Geophys. Res.*, *102*(B1), 591–604.

Langbein, J., K. Breckenridge, and E. Quilty (1993), Sensitivity of crustal deformation instruments to changes in secular rate, *Geophys. Res. Lett.*, *20*(2), 85–88.

Langbein, J., F. Wyatt, H. Johnson, D. Hamann, and P. Zimmer (1995), Improved stability of a deeply anchored geodetic monument, *Geophys. Res. Lett.*, *22*(24), 3533–3536.

Langbein, J., J. R. Murray, and H. A. Snyder (2006), Coseismic and initial postseismic deformation from the 2004, Parkfield, California, earthquake observed by GPS, EDM, creepmeters, and boreholes trainmeters, *Bull. Seismol. Soc. Am.*, *96*, S304–S320.

Mao, A., C. G. A. Harrison, and T. H. Dixon (1999), Noise in GPS coordinate time series, *J. Geophys. Res.*, *104*, 2797–2816.

Menke, W. (1984), *Geophysical Data Analysis: Discrete Inverse Theory*, 260 pp., Academic Press, San Diego, Calif.

Nikolaidis, R. (2002), Observation of geodetic and seismic deformation with the Global Positioning System, Ph.D. thesis, Univ. of Calif., San Diego.

Penna, N. T., M. A. King, and M. P. Stewart (2007), GPS height time series: Short-period origins of spurious long-period signals, *J. Geophys. Res.*, *112*, B02402, doi:10.1029/2005JB004047.

Prawirodirdjo, L., Y. Ben-Zion, and Y. Bock (2006), Observation and modeling of thermoelastic strain in Southern California integrated GPS network daily position time series, *J. Geophys. Res.*, *111*, B02408, doi:10.1029/2005JB003716.

Ray, J. R., T. M. van Dam, Z. Altamimi, and X. Collilieux (2006), Anomalous harmonics in the spectra of GPS position estimates, *Eos Trans. AGU*, *87*(52), Fall Meet. Suppl., Abstract G43A-0985.

Segall, P., and M. Matthews (1997), Time-dependent inversion of geodetic data, *J. Geophys. Res*, *102*, 22,391–22,409.

Wdowinski, S., Y. Bock, J. Zhang, P. Fang, and J. Genrich (1997), Southern California Permanent GPS Geodetic Array: Spatial filtering of daily positions for estimating coseismic and postseismic displacements induced by the 1992 Landers earthquake, *J. Geophys. Res.*, *102*(B8), 18,057–18,070.

Wessel, P., and W. H. F. Smith (1991), Free software helps map and display data, *Eos Trans. AGU*, *72*, 441.

Wilcoxon, F. (1945), Individual comparisons by ranking methods, *Biometrics*, *1*, 80–83.

Williams, S. D. P. (2003), The effect of coloured noise on the uncertainties of rates estimated from geodetic time series, *J. Geod.*, *76*, 483–494.

Williams, S. D. P., Y. Bock, P. Fang, P. Jamason, R. M. Nikolaidis, L. Prawirodirdjo, M. Miller, and D. J. Johnson (2004), Error analysis of continuous GPS time series, *J. Geophys. Res.*, *109*, B03412, doi:10.1029/2003JB002741.

Wyatt, F. K. (1982), Displacements of surface monuments: Horizontal motion, *J. Geophys. Res.*, *87*(B2), 979–989.

Wyatt, F. K. (1989), Displacements of surface monuments: Vertical motion, *J. Geophys. Res.*, *94*(B2), 1655–1664.

Wyatt, F. K., H. Bolton, S. Bralla, and D. C. Agnew (1989), New designs of geodetic monuments for use with GPS, *Eos Trans. AGU*, *70*, 1054.

Zhang, J., Y. Bock, H. Johnson, P. Fang, S. Williams, J. Genrich, S. Wdowinski, and J. Behr (1997), Southern California permanent GPS geodetic array: Error analysis of daily position estimates and site velocities, *J. Geophys. Res.*, *102*(B8), 18,035–18,055.

J. Langbein, U.S. Geological Survey, MS 977, 345 Middlefield Road, Menlo Park, CA 94025, USA. (langbein@usgs.gov)